

Article

# Heavy Metal Removal from Wastewater Using Poly(Gamma-Glutamic Acid)-Based Hydrogel

Fujie Chen <sup>1,2</sup>, Yanbin Zhao <sup>1</sup>, Hang Zhao <sup>1</sup>, Xuan Zhou <sup>3,\*</sup> and Xiuying Liu <sup>1,\*</sup>

<sup>1</sup> School of Chemistry and Chemical Engineering, Wuhan Textile University, Wuhan 430200, China; whcfj@wtu.edu.cn (F.C.)

<sup>2</sup> Hubei Key Laboratory of Biomass Fibers and Eco-Dyeing & Finishing, Wuhan Textile University, Wuhan 430200, China

<sup>3</sup> School of Chemistry and Environmental Engineering, Wuhan Institute of Technology, Wuhan 430205, China

\* Correspondence: hbzhoux@sina.com (X.Z.); liuxiuying@wtu.edu.cn (X.L.)

**Abstract:** The removal of toxic heavy metal ions from wastewater is of great significance in the protection of the environment and human health. Poly(gamma-glutamic acid) (PGA) is a non-toxic, biodegradable, and highly water-soluble polymer possessing carboxyl and imino functional groups. Herein, water-insoluble PGA-based hydrogels were prepared, characterized, and investigated as heavy metal adsorbents. The prepared hydrogels were recyclable and exhibited good adsorption effects on heavy metal ions including Cu<sup>2+</sup>, Cr<sup>6+</sup>, and Zn<sup>2+</sup>. The effects of adsorption parameters including temperature, solution pH, initial concentration of metal ions, and contact time on the adsorption capacity of the hydrogel for Cu<sup>2+</sup> were investigated. The adsorption was a spontaneous and exothermic process. The process followed the pseudo-first-order kinetic model and Langmuir isotherm model, implying a physical and monolayer adsorption. The adsorption mechanisms investigation exhibited that Cu<sup>2+</sup> adsorbed on the hydrogel via electrostatic interactions with anionic carboxylate groups of PGA in addition to the coordination interactions with the –NH groups. Importantly, the PGA hydrogel exhibited good reusability and the adsorption capability for Cu<sup>2+</sup> remained high after five consecutive cycles. The properties of PGA hydrogel make it a potential candidate material for heavy metal ion removal in wastewater treatment.

**Keywords:** heavy metal; adsorption; hydrogel; water treatment; polymer; poly(gamma-glutamic acid)



**Citation:** Chen, F.; Zhao, Y.; Zhao, H.; Zhou, X.; Liu, X. Heavy Metal Removal from Wastewater Using Poly(Gamma-Glutamic Acid)-Based Hydrogel. *Gels* **2024**, *10*, 259. <https://doi.org/10.3390/gels10040259>

Academic Editors: Luca Burratti, Paolo Proposito and Iole Venditti

Received: 2 March 2024

Revised: 5 April 2024

Accepted: 7 April 2024

Published: 11 April 2024



**Copyright:** © 2024 by the authors. Licensee MDPI, Basel, Switzerland. This article is an open access article distributed under the terms and conditions of the Creative Commons Attribution (CC BY) license (<https://creativecommons.org/licenses/by/4.0/>).

## 1. Introduction

Most heavy metal ions, even at low concentrations, are toxic and can have detrimental effects on the environment and human health [1]. Industries such as non-ferrous metallurgical industry, fine chemical, paper, engineering, paint, dye, petrochemical, textile, and pharmaceutical, inevitably lead to wastewater with excess concentration of heavy metals [2–4]. Removal of heavy metals from wastewater is of great significance [5]. A variety of technologies including adsorption, extraction, chemical precipitation, ion exchange, electro dialysis, reverse osmosis, and redox have been developed for the removal [5–11]. For example, Yudaev and Chistyakov systematized the works on the extraction process, the classes of chelating extractants for metals, and the efficiency and selectivity of the extractants in the recovery of various metals from industrial wastewater, soil, spent raw materials, and the separation of metal mixtures [11]. The technology of adsorption is based on the physical or chemical interaction between the adsorbent and the heavy metal ions [5,12–14]. It is widely studied due to the relatively simple operation process, the flexibility in the design of adsorbents, and the high removal efficiencies [5].

The adsorbents are various, and Wang et al. categorized them into biosorbents (e.g., agriculture waste biochar/activated carbon, algae, and bacteria) and abiotic adsorbents (e.g., polymers, microtubes, metal-organic frameworks, minerals, clays, and coal) [6,7,15]. Hydrogels are soft matter with a three-dimensional structure created via the cross-linking

of synthetic or natural polymers. They have superior applications for heavy metal removal, due to their excellent properties, such as high functionality, high porosity, handling, ease of preparation, and easy recovery [16]. Many documents have summarized recent progress in the use of hydrogel adsorbents for the removal of heavy metal ions and focused on the adsorption performances of the hydrogels [16–20]. Developments in the synthesis of hydrogel-based adsorbent materials have also been summarized. Hydrogels are generally synthesized via chemical or physical cross-linking [16,19]. The chemical route of cross-linking can be via free radical polymerization, high-energy irradiation, grafting reactions, and reaction of functional groups. The physical route of cross-linking can be via freeze-thaw, self-assembling, instantaneous gelation, ionotropic gelation, or inverse emulsion method.

Hydrogels function as excellent adsorbents in heavy metal removal processes by binding metal ions with various functional groups in their polymeric networks. The adsorptions rely on physical and chemical interactions, such as electrostatic interaction, coordination interaction, hydrophobic interaction, and ion exchange, depending on the surface functional moieties of hydrogels. According to previous documents, electrostatic interactions are the dominant adsorption force for heavy metal abstraction in various hydrogels [19]. The paramount functional groups in hydrogels for ion adsorption are generally classified into three groups: (a) nitrogen-containing functional groups, such as the amine group ( $-\text{NH}_2$ ), amide group ( $-\text{CONH}$ ), and quaternary ammonium group [ $-\text{N}^+(\text{CH}_3)_3$ ]; (b) oxygen-containing functional groups, such as the hydroxyl ( $-\text{OH}$ ) and carboxyl group ( $-\text{COOH}$ ); and (c) sulfur-containing functional groups, such as the thiol ( $-\text{SH}$ ) and sulfonic acid group ( $-\text{SO}_3\text{H}$ ). Other functional groups include the amidoxime group ( $-\text{C}(\text{NH}_2)=\text{N}-\text{OH}$ ), phosphate-containing functional groups (phosphine, phosphate, and phosphoramidate), and chelating groups such as the nitrogen- and oxygen-containing functional groups present in the aminopolycarboxylic acid structure [19].

Hydrogel-forming polymers include natural polymers such as cellulose [21], chitosan and alginate [17,21–25], and synthetic polymers such as polyvinyl alcohol (PVA) [26], polypyrrole [20], aminated polyacrylonitrile [27], polypyrrole-polyaniline [20], and poly(acrylic acid-co-acrylamide) [16]. Chitosan and alginate-based hydrogels are widely studied for the adsorption of metal ions. Composite hydrogels are also well documented. Alginate and chitosan can be incorporated with other components to prepare hydrogels or nanocomposite materials with different efficiencies to remove metal ions and dyes [17].

$\gamma$ -polyglutamic acid (PGA) is a biodegradable, non-toxic, and highly water-soluble polymer derived from glutamic acid and possesses carboxyl functional groups ( $-\text{COOH}$ ) along the polymer side chains and imino groups ( $-\text{NH}$ ) along the backbones. These functional groups have a high binding affinity for heavy metal ions [14]. However, PGA in aqueous form as an adsorbent faces difficulty in separating the heavy metal-accumulating PGA from water [12,13,28–30]. PGA in the form of nanoparticles can be separated from water; however, to achieve the separation of nanoparticles, ultrafiltration technology using nanomembranes is required [31]. Wang and co-workers reported a hybrid alginate-polyglutamic acid hydrogel for the removal and recovery of rare earths (III) from dilute solution. Doping PGA into calcium alginate can significantly enhance the adsorption capacity and the selectivity of rare earths from non-rare earths. The maximum adsorption capacity obtained for Nd(III) was 1.65 mmol/g [32]. Yin et al. designed a combination of  $\gamma$ -polyglutamic acid, polylysine ( $\epsilon$ -PL), and tannin and prepared a composite PGA-PL-tannin gel. The removal rate of Cr(VI) by this gel exceeded 90% [33].

In this study, we aim to prepare a PGA-based hydrogel that is water-insoluble and recyclable, compared to an aqueous PGA adsorbent. It avoids the problem of difficulty in separating heavy metal-accumulating PGA from water. Its performance in heavy metal removal is investigated. A third-generation polyamidoamine (PAMAM) dendrimer with several terminal amino functional groups that are reactive toward PGA is used as the cross-linking reagent, as shown in Figure 1.  $\text{Cu}^{2+}$  was used as the heavy metal model pollutant. The hydrogel is characterized and the effect of adsorption parameters on adsorption is investigated. The adsorption isotherms, adsorption kinetics, thermodynamics models, and

the possible adsorption mechanism for  $\text{Cu}^{2+}$  ions onto PGA hydrogel are analyzed. The reusability of PGA hydrogel is also explored.

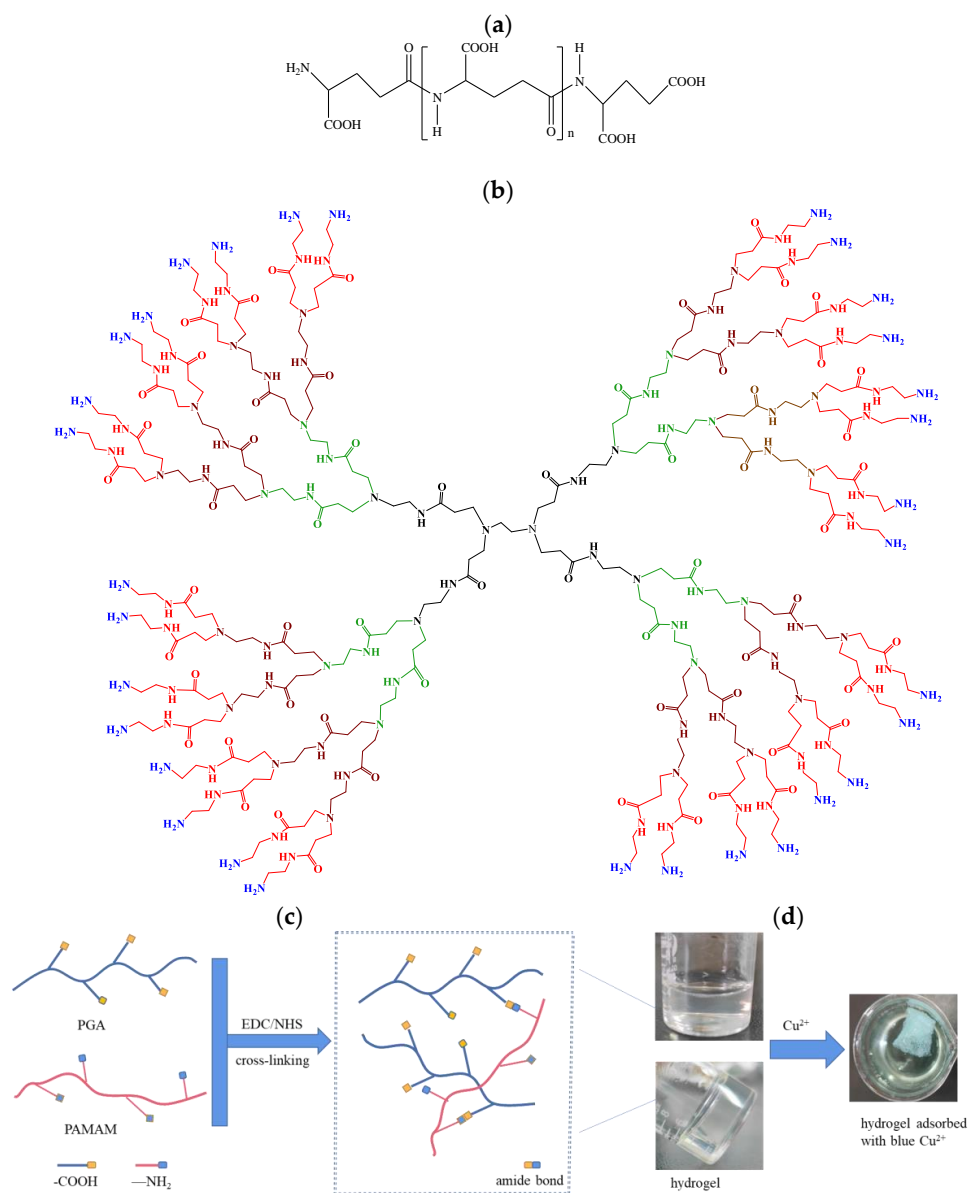


**Figure 1.** (a) Structure of  $\gamma$ -PGA; (b) structure of third-generation PAMAM [34]; (c) preparation scheme of water-insoluble hydrogel by cross-linking between  $\gamma$ -PGA and PAMAM; (d) images of hydrogel before and after adsorption of  $\text{Cu}^{2+}$ .

## 2. Results and Discussion

### 2.1. Characterizations of the Hydrogel

The hydrogel was prepared, and the real image is shown in Figure 2a. The SEM images in Figure 2b,c exhibited that the hydrogel had a porous and regular network structure. The porous structure makes it possible for the metal ions to enter the hydrogel. The network structure indicated that cross-linking was formed between PGA and PAMAM and led to the water-insolubility of the hydrogel. SEM of the hydrogels after adsorption of  $\text{Cu}^{2+}$ ,  $\text{Zn}^{2+}$ , and  $\text{Cr}^{6+}$  ions are shown in Figure 2d–f, which revealed that the hydrogel surfaces were irregular and had lower porosity than the hydrogel before metal ion adsorption. This is because the electrostatic repulsions decline in the network of hydrogels after the anionic groups of the hydrogels absorb the cationic metal ions, as reported by Yang et al. [35]. Another reason is due to metal ions occupying the pores [36]. To confirm the chemical

cross-linking, FTIR of the hydrogel and PGA were compared, as shown in Figure 3. In the infrared spectrum of PGA, the peak at  $3423\text{ cm}^{-1}$  belongs to the stretching vibrations of the carboxylic O–H and imino N–H, and the absorption band at  $1624\text{ cm}^{-1}$  can be assigned to N–H shearing vibration. In contrast to PGA, the corresponding peaks of the hydrogel appear at  $3403\text{ cm}^{-1}$  and  $1644\text{ cm}^{-1}$ , respectively. The peak shifts indicated that part of the –COOH and –NH groups participated in the cross-linking between PGA and PAMAM. The hydrogel exhibits a new strong peak at  $1565\text{ cm}^{-1}$ , which corresponds to the solid N–H peak or N–H shear vibration of secondary amide. In addition, two other new peaks are observed at  $1258$  and  $1080\text{ cm}^{-1}$ , attributable to the stretching vibrations of the C–O and C–N bonds of the secondary amide. These results imply that the amide groups (–NHCO–) formed upon cross-linking. The BET test results showed that the specific surface area of the hydrogel is very small, implying that the specific surface area had little effect on the adsorption of copper ions. The hydrogel was immersed in water for 8 h and it was insoluble in water. As shown in Figure 4, the swelling ratio of the hydrogel reached  $10.53\text{ g/g}$ , indicating the excellent hydrophilicity of the PGA hydrogel. The hydrogels with good swelling properties provided diffusion channels for heavy metal ions, which facilitated the binding of metal ions to the adsorption sites inside the hydrogel materials [37]. Chowdhury et al. reported that the degree of swelling of PVA hydrogels is about 370% and the removal of copper by PVA hydrogels is about  $7\text{ mg/g}$  [38]. According to Romal et al., the swelling capacities of chitosan hydrogel and Mannich base-modified chitosan (CS-MB) hydrogel in unbuffered distilled water after 4 min reached  $25.7\text{ g/g}$  and  $8.09\text{ g/g}$ , respectively. CS-MB hydrogel showed a  $\text{Cu}^{2+}$  adsorption capacity of  $12.0\text{ mg/g}$ . However, no data were provided by them about the adsorption capacity of chitosan hydrogel [39]. However, Dai and co-workers reported that the hydration rate and the copper(II) adsorption capacity of chitosan hydrogel reached 94.07% and  $60\text{ mg/g}$ , respectively [40]. What is more, the water content of the swelling carboxymethylated chitosan (CMC) hydrogel beads is 95.5% and its equilibrium Cu(II) uptake is as high as about  $130\text{ mg/g}$  [41]. Cellulose hydrogel also has a great swelling ability of 4650% and a high adsorption capacity of  $28.4\text{ mg/g}$  for copper ions [37]. In contrast, the swelling ability of the PGA hydrogel is higher than that of PVA, and lower than that of chitosan, CS-MB, cellulose, and CMC.

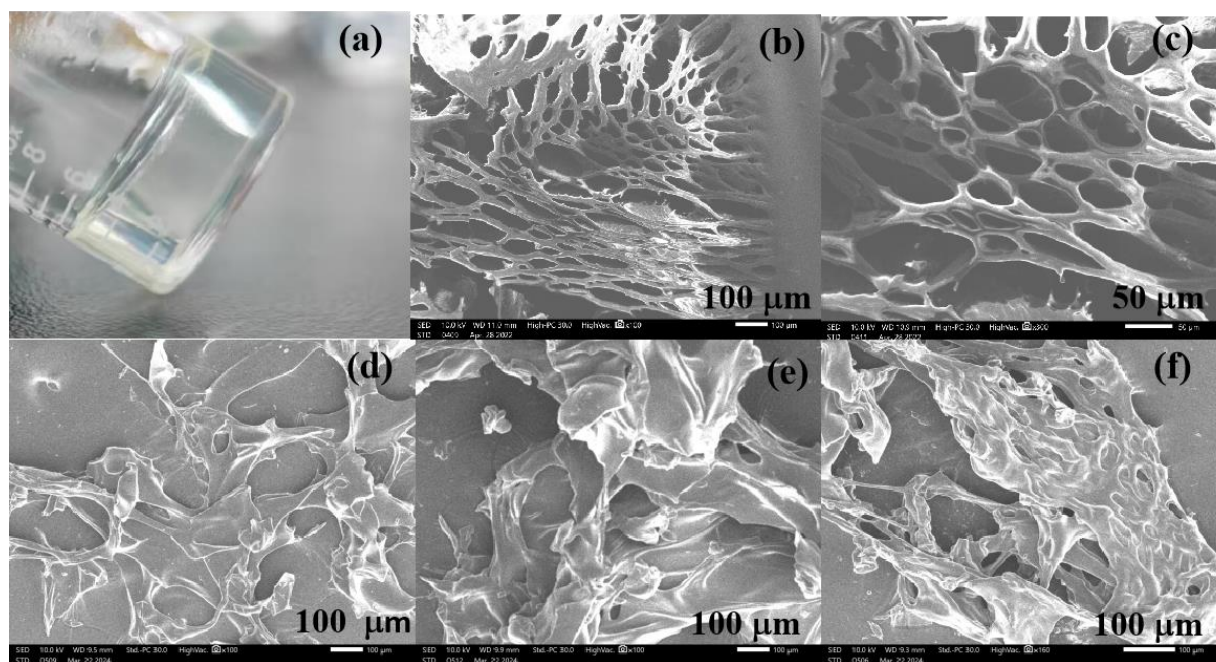


**Figure 2.** (a) Real image of the hydrogels; (b,c) SEM images of the hydrogels before metal ion adsorption under different magnifications; (d–f) SEM images of the hydrogels after adsorption of  $\text{Cu}^{2+}$ ,  $\text{Zn}^{2+}$ , and  $\text{Cr}^{6+}$  ions, respectively.

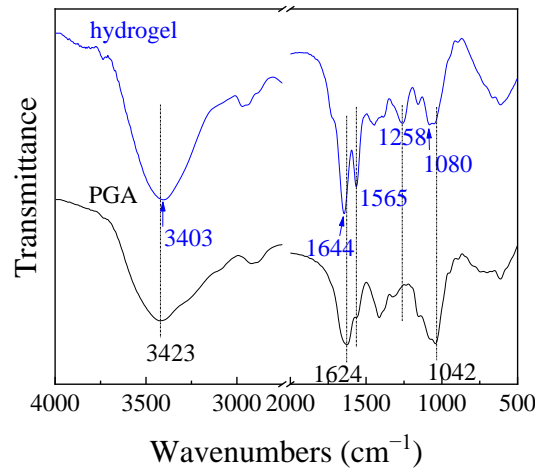


Figure 3. FTIR of PGA and the hydrogel.

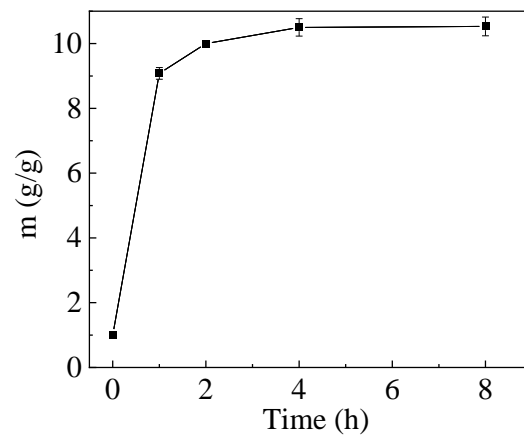


Figure 4. Swelling ratio of the hydrogel.

## 2.2. Adsorption Performance of PGA Hydrogels

### 2.2.1. Adsorption Kinetics

The adsorption capacity of the hydrogel for  $\text{Cu}^{2+}$  with time is shown in Figure 5. It increased rapidly within 2 h, then slowly, and reached its equilibrium value of 8.6 mg/g within 24 h. The value is equivalent to that of polyvinyl alcohol [38] and the composite adsorbent of collodion membrane cross-linked poly- $\gamma$ -glutamic acid [42], and lower than that of PGA in aqueous form as an adsorbent. It is also lower than cellulose and chitosan, which have high swelling capacities. To investigate the mechanism of the adsorption process, the adsorption kinetic data were analyzed using pseudo-first-order and pseudo-second-order models, and the corresponding equations are as follows:

$$Q_t = q_{e1} \times (1 - e^{-k_1 t}) \quad (1)$$

$$Q_t = \frac{q_{e2}^2 k_2 t}{1 + q_{e2} k_2 t} \quad (2)$$

where  $Q_t$  (mg/g) represents the adsorption capacity of the hydrogel at time  $t$ .  $q_{e1}$  and  $q_{e2}$  ( $\text{mg g}^{-1}$ ) are the equilibrium adsorption capacity of the hydrogels calculated by pseudo-first-order and pseudo-second-order kinetic models, respectively.  $k_1$  ( $\text{min}^{-1}$ ) and  $k_2$  ( $\text{g mg}^{-1} \text{min}^{-1}$ ) represent the adsorption rate constants of the pseudo-first-order model and pseudo-second-order model, respectively.

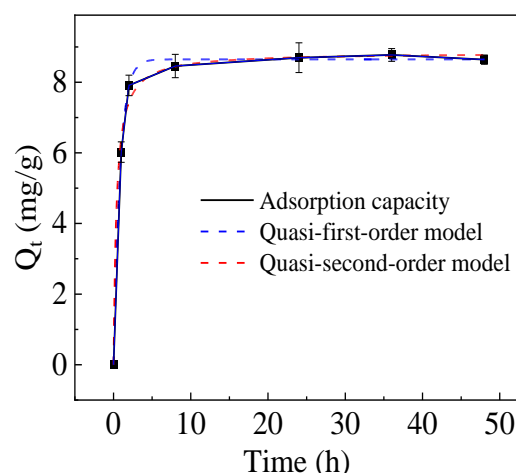


**Figure 5.** Adsorption kinetic of  $\text{Cu}^{2+}$  on the hydrogel.

The fitted curves of the adsorption kinetic equation and the fitted parameters are demonstrated in Figure 5 and Table 1, respectively. Based on the correlation coefficients ( $R^2$ ) of the equations, the adsorption process followed the pseudo-first-order ( $R^2 = 0.9989$ ) kinetic better than the pseudo-second-order kinetic ( $R^2 = 0.9261$ ), illustrating that physical adsorption is dominant in the adsorption process [43]. In addition, the theoretical equilibrium adsorption capacity calculated by the quasi-first-order model ( $q_{e1}$ ) was closer to the experimental equilibrium adsorption capacity ( $Q_e$ ) than that of the quasi-second-order model ( $q_{e2}$ ), confirming that the adsorption of  $\text{Cu}^{2+}$  onto the hydrogel was controlled by the physical adsorption [43].

**Table 1.** Kinetic parameters of pseudo-first-order and pseudo-second-order models for  $\text{Cu}^{2+}$  adsorption onto the hydrogel.

$Q_e$ (mg/g)	Pseudo-First-Order			Pseudo-Second-Order		
	$q_{e1}$ (mg g <sup>-1</sup> )	$k_1$ (min <sup>-1</sup> )	$R^2$	$q_{e2}$ (mg g <sup>-1</sup> )	$k_2$ (g mg <sup>-1</sup> min <sup>-1</sup> )	$R^2$
$8.6 \pm 0.1$	8.64	$9.04 \times 10^{-2}$	0.9989	8.84	0.2974	0.9261

### 2.2.2. Adsorption Isotherm

To further study the adsorption mechanism, the adsorption isotherm for  $\text{Cu}^{2+}$  adsorption on hydrogel was investigated. As shown in Figure 6a,  $Q_e$  increased with the increase in initial  $\text{Cu}^{2+}$  concentration. The Langmuir and Freundlich isotherms that are the most commonly used are applied to interpret the adsorption behavior. Equations (3) and (4) are the formulae for the Langmuir and Freundlich models.

$$Q_e = \frac{K_L Q_m C_e}{1 + K_L C_e} \quad (3)$$

$$Q_e = K_F C_e^{\frac{1}{n}} \quad (4)$$

where  $Q_m$  (mg g<sup>-1</sup>) is the theoretical maximum adsorption capacity;  $K_L$  (L mg<sup>-1</sup>) and  $K_F$  (L<sup>n</sup> mg<sup>n-1/n</sup> g<sup>-1</sup>) are Langmuir and Freundlich constants, respectively;  $1/n$  is the surface heterogeneity of the adsorbent. The fitted curves and the parameters obtained from two isotherm models are shown in Figure 6b and Table 2, respectively. The adsorption process is better suited to the Langmuir model with higher  $R^2$  values ( $R^2 = 0.9863$ ) than the Freundlich isotherm ( $R^2 = 0.9781$ ), implying that the adsorption of copper ions by hydrogel is mainly through single-layer adsorption [44].

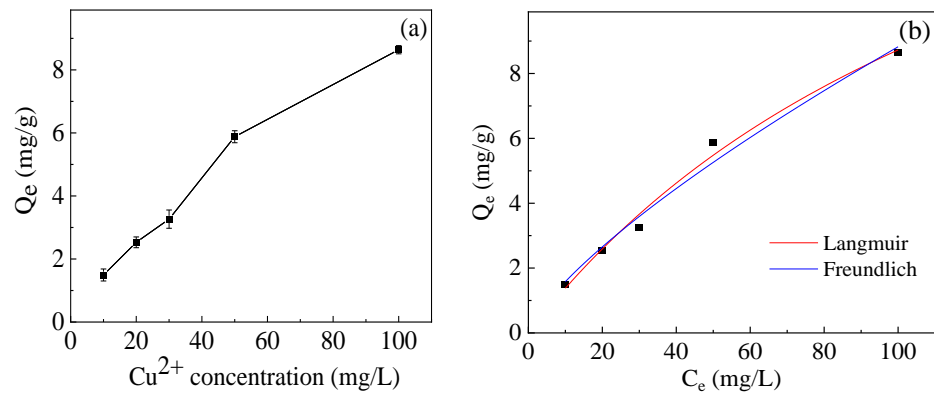


**Figure 6.** (a) Adsorption isotherm of  $\text{Cu}^{2+}$  and (b) fitted curves of Langmuir and Freundlich adsorption isotherm models.

**Table 2.** Isotherm parameters of  $\text{Cu}^{2+}$  adsorption onto hydrogel.

Langmuir Model			Freundlich Model		
$Q_m$ ( $\text{mg g}^{-1}$ )	$K_L$ ( $\text{L mg}^{-1}$ )	$R^2$	$K_F$ ( $\text{L}^n \text{mg}^{n-1/n} \text{g}^{-1}$ )	$1/n$	$R^2$
21.41	0.0069	0.9863	0.2833	0.7466	0.9781

### 2.2.3. Adsorption Thermodynamics

The thermodynamics study is helpful to understand the adsorption process better; the thermodynamic parameters from the experiment at different temperatures are shown in Table 3. The negative value of  $\Delta H^0$  of adsorption  $\text{Cu}^{2+}$  represents that the adsorption process is exothermic. The negative values of  $\Delta G^0$  at all tested temperatures represent the spontaneous nature of adsorption. In addition, the increase in  $\Delta G^0$  with the increase in temperature exhibits that the adsorption becomes more favorable at the lower temperature.

**Table 3.** Thermodynamic parameters for  $\text{Cu}^{2+}$  adsorption onto hydrogel.

$\Delta H^0$ ( $\text{kJ}\cdot\text{mol}^{-1}$ )	$\Delta S^0$ ( $\text{kJ}\cdot\text{mol}^{-1}\cdot\text{K}^{-1}$ )	$\Delta G^0$ ( $\text{kJ}\cdot\text{mol}^{-1}$ )			$R^2$
		298 K	318 K	328 K	
-1792.42	-5.4252	-175.70	-67.20	-12.95	0.9999

### 2.2.4. Effect of Solution pH on Adsorption

As shown in Figure 7, the adsorption capacity of hydrogel for  $\text{Cu}^{2+}$  increases with the increase in solution pH from 3 to 7. While the solution pH continues to increase and the value is over 7, the precipitation of  $\text{Cu}(\text{OH})_2$  occurs. At higher solution pH ( $\text{pH} > \text{pK}_a \sim 4$ ),  $-\text{COOH}$  groups in PGA polymer side chains will ionize to form the anionic carboxylate ( $-\text{COO}^-$ ) groups because the  $\text{pK}_a$  of PGA is 4.09 [45]. The negatively charged  $-\text{COO}^-$  groups are significantly stronger ligands than  $-\text{COOH}$  for metal ion binding [46]. Therefore, the increased adsorption capacity was mainly attributed to the electrostatic interaction between  $-\text{COO}^-$  and the cationic ion  $\text{Cu}^{2+}$ . In addition, at higher solution pH, the imino  $-\text{NH}$  groups in the polymer backbone are deprotonated. The deprotonated  $-\text{NH}$  is an electron-donating group that had higher adsorption affinity towards the cationic ion  $\text{Cu}^{2+}$  and adsorbed  $\text{Cu}^{2+}$  via the coordination interaction, compared to the protonated  $-\text{NH}_2^+$  group [1].

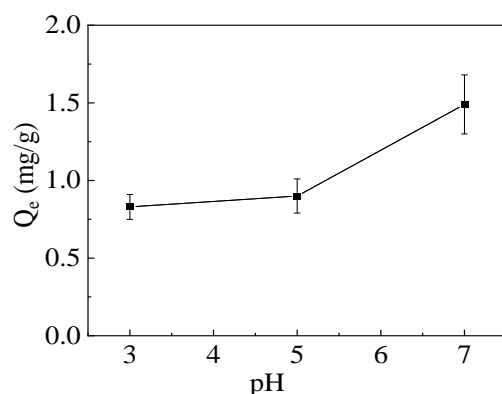


**Figure 7.** Effect of solution pH on adsorption.

#### 2.2.5. Effect of the Mass of the Adsorbent on Adsorption

The effect of the mass of the adsorbent on the adsorption capacity is shown in Figure 8. The adsorption capacity decreased with the increase in adsorbent weight, consistent with  $\beta$ -cyclodextrin-based adsorbent and poly(methacrylic acid)/zeolite hydrogel composites [27,47]. This is possibly because the added adsorbent provided excessive active groups beyond the capacity to be accepted by the heavy metal ions, leading to a reduced number of ions adsorbed onto the unit weight of the adsorbent. While the hydrogel dosage is between 0.5 and 0.6 g, the change in adsorption capacity is relatively small. Therefore, the dosage of hydrogel in this work is 0.5 g.

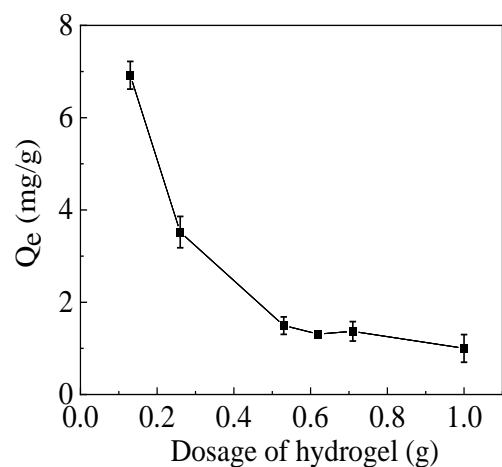


**Figure 8.** Effect of the adsorbent dosage on adsorption.

#### 2.2.6. Reusability

The PGA hydrogel absorbed with  $\text{Cu}^{2+}$  was regenerated by desorption of  $\text{Cu}^{2+}$  with ammonia water as the desorbent. Adsorption-desorption cycles were carried out to evaluate the reusability of the hydrogel for  $\text{Cu}^{2+}$  removal. The adsorption capacity of the first adsorption process was set as 100%, and the adsorption capacity ratio of each cycle versus the first cycle was calculated for the reusability evaluation [43]. As shown in Figure 9, the ratio decreased gradually, but it remained at 95% in the first run and remained at 78.5% in the fifth run, indicating that the hydrogels had excellent reusability. The reuse of the PGA hydrogel in metal ion removal reduces resource consumption and makes the material cost-effective, in contrast to the non-renewable PGA aqueous solution adsorbent [13].

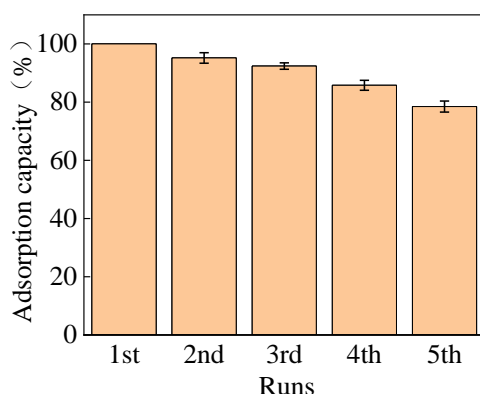


**Figure 9.** Reusability of the hydrogel for Cu<sup>2+</sup> adsorption.

### 2.2.7. Adsorption of Other Heavy Metal Cations

The adsorptions of Zn<sup>2+</sup> and Cr<sup>6+</sup> by the hydrogel were also investigated. The experiment was carried out by immersing 0.03 g hydrogel in Zn<sup>2+</sup> (200 mg/L, pH 7) and Cr<sup>6+</sup> (30 mg/L, pH 7) solution at 25 °C. As shown in Figure 10a,b, the adsorption capacities are 43.2 mg/g and 17.4 mg/g, respectively, illustrating the applicability of the hydrogel for the removal of Zn<sup>2+</sup> and Cr<sup>6+</sup>.

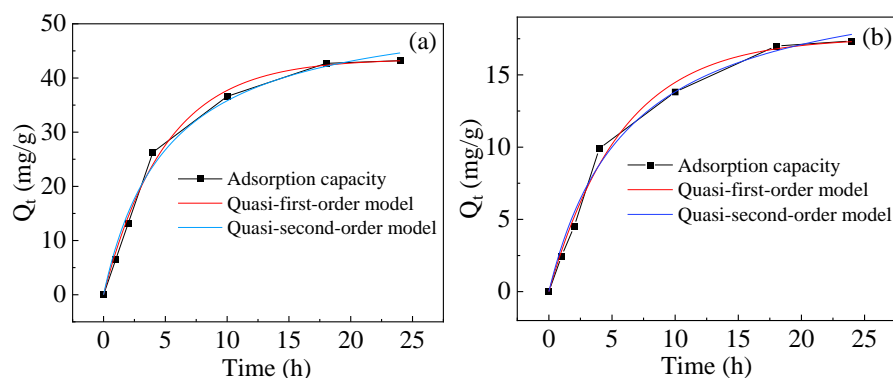


**Figure 10.** Adsorption kinetic of (a) Zn<sup>2+</sup> and (b) Cr<sup>2+</sup> on the hydrogel.

The fitted curves of the adsorption kinetic equation and the fitted parameters are shown in Figure 10 and Table 4, respectively. Physical adsorption is also dominant in the adsorption process, because the adsorption process followed the pseudo-first-order kinetic better than the pseudo-second-order kinetic, based on the correlation coefficients ( $R^2$ ) of the equations.

**Table 4.** Kinetic parameters of pseudo-first-order and pseudo-second-order models for the adsorption of Zn<sup>2+</sup> and Cr<sup>6+</sup> onto the hydrogels.

Metal Ions	$Q_e$ (mg/g)	Pseudo-First-Order			Pseudo-Second-Order		
		$qe1$ (mg g <sup>-1</sup> )	$k_1$ (min <sup>-1</sup> )	$R^2$	$qe2$ (mg g <sup>-1</sup> )	$k_2$ (g mg <sup>-1</sup> min <sup>-1</sup> )	$R^2$
Zn <sup>2+</sup>	43.2	43.52	0.2011	0.9938	54.1	0.0035	0.9881
Cr <sup>6+</sup>	17.35	17.57	0.1735	0.9910	22.41	0.0071	0.9883

The adsorption isotherm of Zn<sup>2+</sup> and Cr<sup>2+</sup> and fitted curves of the Langmuir and Freundlich adsorption isotherm models are shown in Figure 11. The parameters from two isotherm models are shown in Table 5, respectively. Based on the  $R^2$  values, the adsorption process is better suited to the Langmuir model than the Freundlich isotherm.

Therefore, the adsorptions of  $\text{Zn}^{2+}$  and  $\text{Cr}^{2+}$  by hydrogel are also mainly through single-layer adsorption.

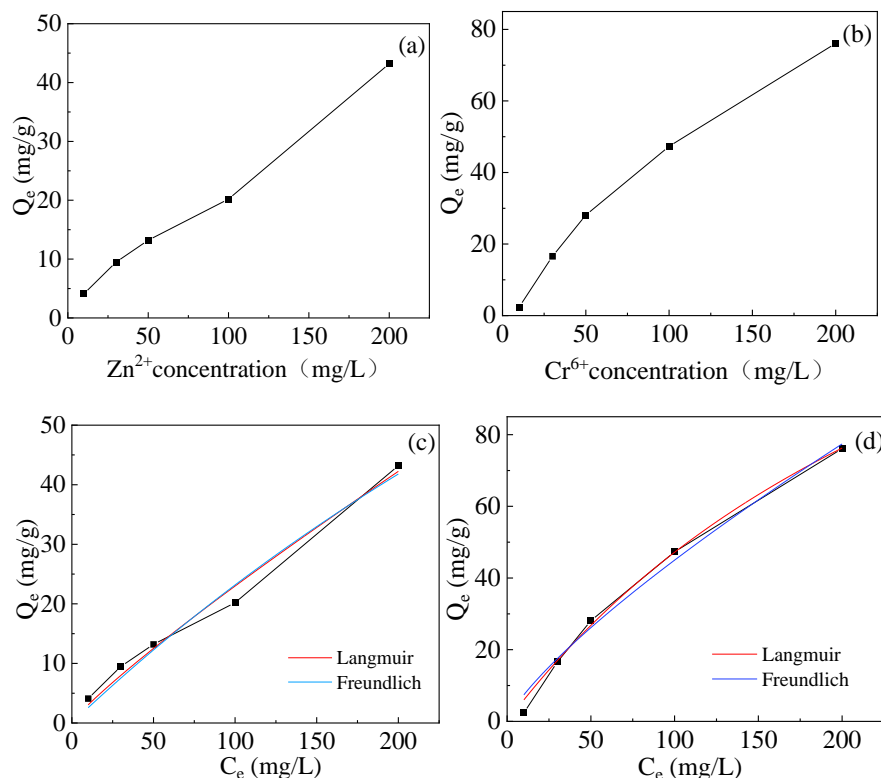


**Figure 11.** Adsorption isotherm of (a)  $\text{Zn}^{2+}$  and (b)  $\text{Cr}^{2+}$  and fitted curves of Langmuir and Freundlich adsorption isotherm models of (c)  $\text{Zn}^{2+}$  and (d)  $\text{Cr}^{2+}$ .

**Table 5.** Isotherm parameters of  $\text{Zn}^{2+}$  and  $\text{Cr}^{2+}$  adsorption onto hydrogels.

Heavy Metal Ions	Langmuir Model			Freundlich Model		
	$Q_m$ ( $\text{mg g}^{-1}$ )	$K_L$ ( $\text{L mg}^{-1}$ )	$R^2$	$K_F$ ( $\text{L}^n \text{mg}^{n-1/n} \text{g}^{-1}$ )	$1/n$	$R^2$
$\text{Zn}^{2+}$	212.3	0.0012	0.9994	0.4039	0.8774	0.9819
$\text{Cr}^{6+}$	198.63	0.0031	0.9939	1.2225	0.7829	0.9850

The thermodynamic parameters from the adsorption experiment of  $\text{Zn}^{2+}$  and  $\text{Cr}^{2+}$  at different temperatures are demonstrated in Table 6. The positive value of  $\Delta H^0$  of adsorption indicates that the adsorption process is endothermic. The negative values of  $\Delta G^0$  represent the spontaneous nature of adsorption.

**Table 6.** Thermodynamic parameters for metal ion adsorption onto hydrogel.

Heavy Metal Ions	$\Delta H^0$ ( $\text{kJ}\cdot\text{mol}^{-1}$ )	$\Delta S^0$ ( $\text{kJ}\cdot\text{mol}^{-1}\cdot\text{K}^{-1}$ )	$\Delta G^0$ ( $\text{kJ}\cdot\text{mol}^{-1}$ )			$R^2$
			298 K	308 K	318 K	
$\text{Zn}^{2+}$	0.12238	0.00046	−0.0147	−0.0193	−0.024	0.9863
$\text{Cr}^{6+}$	0.3635	0.0013	−0.0477	−0.0615	−0.0729	0.9999

### 2.3. Adsorption Mechanism

To explore the adsorption mechanism, FTIRs of the hydrogels before and after the adsorption of  $\text{Cu}^{2+}$  were compared and are shown in Figure 12. Upon adsorption, the peaks at  $3403$  and  $1644 \text{ cm}^{-1}$  attributable to O–H and N–H vibrations shifted to  $3431$  and  $1638 \text{ cm}^{-1}$ , respectively, indicating that the carboxylic hydroxyl ( $-\text{COOH}$ ) and  $-\text{NH}$

functional groups participated in the adsorption of copper ions. In addition, the peak at  $1565\text{ cm}^{-1}$  belonging to the N–H vibration, as well as the peaks at  $1258$ ,  $1158$ , and  $1080\text{ cm}^{-1}$  attributable to the stretching vibrations of C–O or C–N, weakened after the adsorption process, confirming that –COOH and –NH groups in the hydrogel were the main sites of  $\text{Cu}^{2+}$  adsorption. This is consistent with the results of the effect of solution pH on the adsorption capacity. The electron-donating –NH groups adsorb  $\text{Cu}^{2+}$  via the coordination interactions and –COO<sup>−</sup> via electrostatic interactions.

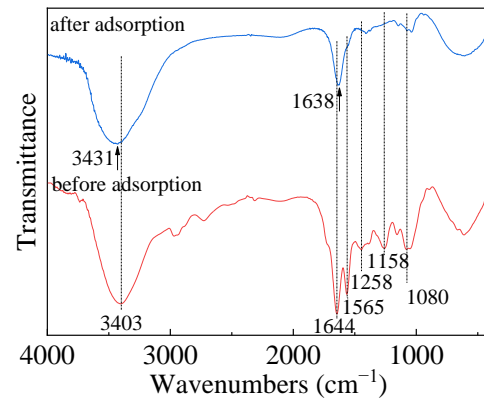


**Figure 12.** FTIR of the hydrogels before and after the adsorption.

To explore the adsorption mechanism further, XPS was also used to detect the chemical bonds on the hydrogel surface. Figure 13a shows the XPS survey scans and Figure 13b–e exhibit the high-resolution scans of C1s, O1s, N1s, and Cu2p spectra with their respective deconvolutions. In the C1s spectrum of hydrogel before adsorption, the peaks centered at 283.9, 285.6, and 288.1 eV are related to C–C/C–H bonds, C–NH, and C=O, respectively [48]. After adsorption, the peaks slightly shifted to 284.2, 285.7, and 287.2 eV, respectively, possibly due to the interaction with  $\text{Cu}^{2+}$  [29]. In the O1s spectrum of the hydrogel before adsorption, the peaks centered at 532.6 and 531.1 eV are related to O=C–N and O=C–OH, respectively [30,49]. After adsorption, the spectrum showed a new peak at 532.1 eV, attributed to the transformation of the carboxylic groups (–COOH) to carboxylates (–COO<sup>−</sup>) by the adsorption of  $\text{Cu}^{2+}$  [30]. This indicates that  $\text{Cu}^{2+}$  adsorbed on the hydrogel via the electrostatic interactions with –COO<sup>−</sup> [1]. The N1s spectra of the hydrogel before adsorption exhibited peaks centered at 399.0 eV assigned to the N–H groups [29,49]. After adsorption, a peak centered at 401.2 eV belonging to –NH<sub>2</sub><sup>+</sup> appeared [29,49]. The H<sup>+</sup> for protonation of –NH comes from the –COOH group on PGA and the deprotonated –COO<sup>−</sup> anion binds to the  $\text{Cu}^{2+}$  ion, consistent with the results of the O1s spectra. As shown in Figure 13e, two peaks centered at 932.3 and 952.0 eV associated with Cu 2p<sub>3/2</sub> and Cu 2p<sub>1/2</sub> [50], respectively, appeared after adsorption, which was not observed before the adsorption. This indicates that  $\text{Cu}^{2+}$  was captured into the hydrogel.

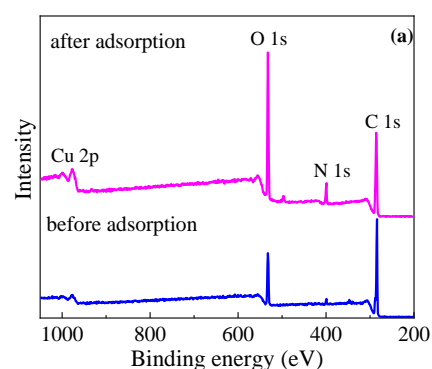


**Figure 13.** Cont.

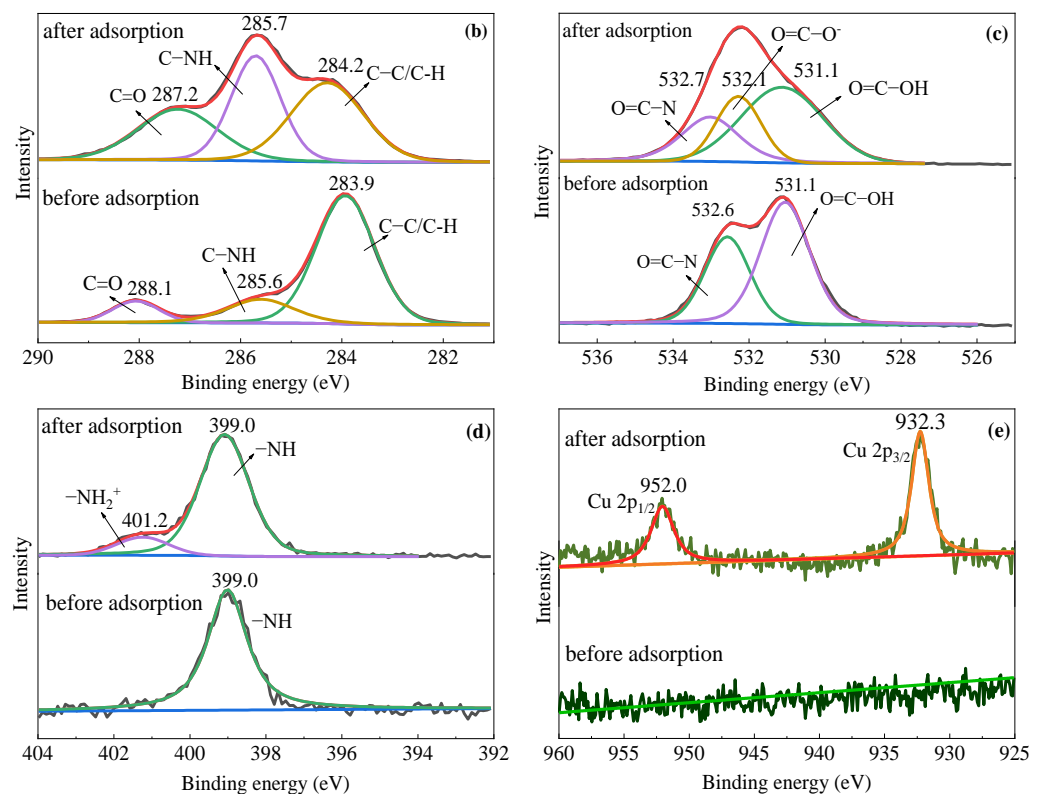


**Figure 13.** XPS spectra of PGA before and after metal adsorption: (a) survey spectra, (b) C1s spectra, (c) O1s spectra, (d) N1s spectra, and (e) Cu2p spectra.

### 3. Conclusions

A water-insoluble and recyclable PGA-based hydrogel was prepared for heavy metal removal. The hydrogel form of adsorbent made the adsorption operation simple. The adsorption capacity of the hydrogel for Cu<sup>2+</sup> is 8.6 mg/g. It is similar to that of PVA and much lower than that of chitosan, modified chitosan, and cellulose. The adsorption is a single-layer physisorption and Cu<sup>2+</sup> is adsorbed on the hydrogel via electrostatic interactions with -COO<sup>-</sup> in addition to the coordination interactions with the -NH of PGA. Therefore, the adsorption capacity of the hydrogel for Cu<sup>2+</sup> increased with the increase in solution pH with more -COO<sup>-</sup> and the deprotonated -NH groups. The adsorption process is spontaneous and exothermic, and a low temperature is favorable to the process. The PGA-based hydrogel had good reusability and it made the hydrogel a cost-effective adsorption material for heavy metal ion removal from wastewater. However, the adsorption capacity of the PGA hydrogel shows a decrease in removal efficiency with cycles. In addition, there are other limitations; for example, the application of hydrogel-based adsorbent materials in heavy metal removal is limited to lab scale. Further research is required to scale up for a large-scale application. In addition, this research lacks the research of selectivity of the sorbent concerning copper in the presence of zinc, chromium, and other heavy metals. The present research is also confined to the removal of three kinds of heavy metal ions. More research should be undertaken targeting multiple heavy metals.

### 4. Materials and Methods

#### 4.1. Materials and Instruments

PGA (molecular weight 700,000) was purchased from Shanghai Yika Biotechnology Co., Ltd. (Shanghai, China). PAMAM was obtained from Weihai Chenyuan Molecular New Materials Co., Ltd. (Weihai, China). N-(3-dimethylaminopropyl)-N-ethylcarbodiimide hydrochloride (EDC) was obtained from Hebei Bailingwei Ultrafine Materials Co., Ltd. (Langfang, China). Sodium diethyldithiocarbamate trihydrate (SDDT) came from Shanghai

Aladdin Biochemical Technology Corporation (Shanghai, China). N-hydroxysuccinimide (NHS), potassium bromide (KBr), ammonia water, and copper chloride ( $\text{CuCl}_2$ ) were all purchased from Sinopharm Chemical Reagents Co., Ltd. (Shanghai, China). Deionized water was used in the experiment.

#### 4.2. Characterizations

The absorbances of  $\text{Cu}^{2+}$  solutions were measured using an ultraviolet-visible (UV-Vis) spectrophotometer (TU-1950, Beijing Puxi General Instrument Co., Ltd., Beijing, China). The concentrations of  $\text{Zn}^{2+}$  and  $\text{Cr}^{6+}$  solutions were determined by an inductively coupled plasma spectrometer (ICP2060T, Jiangsu Skyray Instrument Co., Ltd., Kunshan, China). Fourier transform infrared spectrum (FTIR) was recorded by an infrared spectrometer (FTIR-650, Tianjin Gangdong Science and Technology Development Co., Ltd., Tianjin, China). The surface morphologies of hydrogels were examined by scanning electron microscope (SEM) (ZEISS Gemini 300, China Academy of Sciences Brain Science and Intelligent Technology Innovation Center, Shanghai, China). X-ray photoelectron spectroscopy (XPS) was performed using a Thermo Scientific K-Alpha spectrometer (Thermo Fisher Scientific Inc., Waltham, MA, USA). The surface area was determined with the Brunauer-Emmett-Teller (BET) method using a fully automatic specific surface area analyzer (APSP 2460, Micromeritics Instrument Corp., Norcross, GA, USA).

#### 4.3. Preparation of Hydrogel

Firstly, PGA aqueous solution was obtained by dissolving 0.15 g PGA in 3 mL water by stirring for 30 min using an ultrasonic instrument. Secondly, the PAMAM aqueous solution was prepared by adding 100  $\mu\text{L}$  of 0.21 g/mL PAMAM methanol solution into 1 mL water and shaking. Thirdly, PGA and PAMAM solutions were mixed evenly by stirring for 30 min. Finally, 1 mL aqueous solution containing 0.08 g EDC and 0.08 g NHS was added to the mixture and the stirring continued until the hydrogel formed. The hydrogel was freeze-dried for use.

#### 4.4. Determination of $\text{Cu}^{2+}$ Concentration

SDDT is used as a chromophoric reagent for UV-Vis spectrophotometric determination of  $\text{Cu}^{2+}$  concentration [43]. Briefly, 1 mL SDDT solution (0.2%, *w/w*) was added to 5 mL  $\text{Cu}^{2+}$  solutions of different concentrations (0, 0.5, 1.0, 2.0, 4.0, 6.0, 8.0, 10.0 mg/L). The solution absorbance at 447 nm was recorded to create a standard curve of absorbance against concentration. The samples of unknown concentrations were tested for their absorbance and the concentrations were determined using the standard curve.

#### 4.5. Adsorption Kinetics

The static adsorption of  $\text{Cu}^{2+}$  by the hydrogel was carried out by immersing  $0.5 \text{ g} \pm 5 \text{ mg}$  hydrogel (a cylindrical body with a diameter of 10 mm and a height of 15 mm) into 100 mL  $\text{Cu}^{2+}$  solution (100 mg/L, pH 7) at 25 °C. At a given time interval, the solution absorbance at 447 nm was measured to determine the residual  $\text{Cu}^{2+}$  concentration. The adsorption capacity of the hydrogel at time  $t$  ( $Q_t$ , mg/g) and equilibrium ( $Q_e$ , mg/g) were calculated using Equations (5) and (6), respectively.

$$Q_t = \frac{(C_0 - C_t)V}{m} \quad (5)$$

$$Q_e = \frac{(C_0 - C_e)V}{m} \quad (6)$$

where  $C_0$  (mg/L) and  $C_e$  (mg/L) represent the initial and equilibrium concentration of  $\text{Cu}^{2+}$ , respectively;  $C_t$  (mg/L) is the residual  $\text{Cu}^{2+}$  concentration at time  $t$ ;  $V$  (L) represents the solution volume;  $m$  (g) is the adsorbent weight.

#### 4.6. Adsorption Isotherms

Quantities of  $0.5 \text{ g} \pm 5 \text{ mg}$  hydrogel were immersed in 100 mL  $\text{Cu}^{2+}$  solution of different concentrations (10~100 mg/L, pH 7) at 25 °C for the static adsorption of  $\text{Cu}^{2+}$  and allowed to reach a state of adsorption equilibrium.

#### 4.7. Adsorption Thermodynamics

Quantities of  $0.5 \text{ g} \pm 5 \text{ mg}$  hydrogel were put into 100 mL  $\text{Cu}^{2+}$  solution (100 mg/L, pH 7), at 25 °C, 35 °C, and 45 °C, for the static adsorption of  $\text{Cu}^{2+}$  to an adsorption equilibrium. The experimental data were analyzed to calculate the thermodynamic parameters according to thermodynamic Equations (7)–(10), respectively.

$$\Delta G = -RT \ln K \quad (7)$$

$$\Delta G = \Delta H - T\Delta S \quad (8)$$

$$\ln K = -\frac{\Delta H}{R} \cdot \frac{1}{T} + \frac{\Delta S}{R} \quad (9)$$

$$K = \frac{Q_e}{C_e} \quad (10)$$

where  $\Delta G$  (J/mol),  $\Delta H$  (J/mol), and  $\Delta S$  represent the changes in Gibbs free energy, enthalpy, and entropy, respectively.  $K$  (L/mol) is the equilibrium constant and  $R$  represents the universal gas constant.  $T$  (K) is the absolute temperature.

#### 4.8. Effect of the Solution pH on Adsorption

To investigate the effect of solution pH on  $\text{Cu}^{2+}$  adsorption,  $0.5 \text{ g} \pm 5 \text{ mg}$  hydrogel was immersed in 100 mL  $\text{Cu}^{2+}$  solutions at different pH (10 mg/L, pH 3~7) at 25 °C for the static adsorption of  $\text{Cu}^{2+}$  to a state of adsorption equilibrium.

#### 4.9. Effect of the Mass of the Adsorbent on Adsorption

To investigate the effect of the mass of the adsorbent on  $\text{Cu}^{2+}$  adsorption, various gram quantities of hydrogel were immersed in 100 mL  $\text{Cu}^{2+}$  solutions (10 mg/L, pH 7) at 25 °C for the static adsorption of  $\text{Cu}^{2+}$  to a state of adsorption equilibrium.

#### 4.10. Reusability

To investigate the recyclability performance of the adsorbent, the hydrogel adsorbed with  $\text{Cu}^{2+}$  was recovered from the solution and desorbed with 0.1 mol/L ammonia solution for 4 h for regeneration. The hydrogel was then treated with the deionized water until neutrality for the next adsorption process.

#### 4.11. Swelling Behavior of the Hydrogels

A quantity of 0.36 g hydrogel was immersed in 100 mL water until reaching a swelling equilibrium; the swelling ratio ( $W$ ) of the hydrogel was calculated according to Equation (11).

$$W = \frac{m_s}{m_d} \quad (11)$$

where  $m_s$  (g) and  $m_d$  (g) are the weights of the swollen and freeze-dried hydrogel, respectively.

**Author Contributions:** Conceptualization, writing—review and editing, and funding acquisition, X.L.; software, methodology, investigation, and writing—original draft preparation, Y.Z.; validation, H.Z.; resources, X.Z.; supervision and project administration, F.C. All authors have read and agreed to the published version of the manuscript.

**Funding:** This work was supported by the Hubei Key Laboratory of Biomass Fibers & Eco-Dyeing & Finishing (Wuhan Textile University) (STRZ202213).

**Institutional Review Board Statement:** Not applicable.

**Informed Consent Statement:** Not applicable.

**Data Availability Statement:** Data are contained within the article.

**Conflicts of Interest:** The authors declare no conflicts of interest.

## References

1. Tang, S.; Yang, J.; Lin, L.; Peng, K.; Chen, Y.; Jin, S.; Yao, W. Construction of physically crosslinked chitosan/sodium alginate/calcium ion double-network hydrogel and its application to heavy metal ions removal. *Chem. Eng. J.* **2020**, *393*, 124728. [[CrossRef](#)]
2. Izydorzyc, G.; Mikula, K.; Skrzypczak, D.; Moustakas, K.; Witek-Krowiak, A.; Chojnacka, K. Potential environmental pollution from copper metallurgy and methods of management. *Environ. Res.* **2021**, *197*, 111050. [[CrossRef](#)]
3. Wang, H.; Chen, N.; Cui, Y.; Liu, Y. Removal of copper ions from wastewater: A Review. *Int. J. Environ. Res. Public Health* **2023**, *20*, 3885. [[CrossRef](#)]
4. Rehman, M.; Liu, L.; Wang, Q.; Saleem, M.H.; Bashir, S.; Ullah, S.; Peng, D. Copper environmental toxicology, recent advances, and future outlook: A review. *Environ. Sci. Pollut. Res.* **2019**, *26*, 18003–18016. [[CrossRef](#)]
5. Shen, C.; Zhao, Y.; Li, W.; Yang, Y.; Liu, R.; Morgen, D. Global profile of heavy metals and semimetals adsorption using drinking water treatment residual. *Chem. Eng. J.* **2019**, *372*, 1019–1027. [[CrossRef](#)]
6. Bayuo, J.; Rwiza, M.J.; Sillanpää, M.; Mtei, K.M. Removal of heavy metals from binary and multicomponent adsorption systems using various adsorbents—A systematic review. *RSC Adv.* **2023**, *13*, 13052–13093. [[CrossRef](#)]
7. Wang, J.; Guo, X. Adsorption kinetics and isotherm models of heavy metals by various adsorbents: An overview. *Crit. Rev. Environ. Sci. Technol.* **2023**, *53*, 1837–1865. [[CrossRef](#)]
8. Rajendran, S.; Priya, A.K.; Kumar, P.S.; Hoang, T.K.A.; Sekar, K.; Chong, K.Y.; Khoo, K.S.; Ng, H.S.; Show, P.L. A critical and recent developments on adsorption technique for removal of heavy metals from wastewater—A review. *Chemosphere* **2022**, *303*, 135146. [[CrossRef](#)]
9. Tran, N.N.; Escrivà-Gelonch, M.; Sarafranz, M.M.; Pho, Q.H.; Sagadevan, S.; Hessel, V. Process technology and sustainability assessment of wastewater treatment. *Ind. Eng. Chem. Res.* **2023**, *62*, 1195–1214. [[CrossRef](#)]
10. Zhang, T.; Wang, F.; Zhou, B. Microbial-Based Heavy Metal Bioremediation: Toxicity and eco-friendly approaches to heavy metal decontamination. *Appl. Sci.* **2023**, *13*, 8439. [[CrossRef](#)]
11. Yudaev, P.; Chistyakov, E. Chelating Extractants for Metals. *Metals* **2022**, *12*, 1275. [[CrossRef](#)]
12. Peng, Y.-P.; Chang, Y.-C.; Chen, K.-F.; Wang, C.-H. A field pilot-scale study on heavy metal-contaminated soil washing by using an environmentally friendly agent—Poly- $\gamma$ -glutamic acid ( $\gamma$ -PGA). *Environ. Sci. Pollut. Res.* **2020**, *27*, 34760–34769. [[CrossRef](#)]
13. Mark, S.S.; Crusberg, T.C.; DaCunha, C.M.; Iorio, A.A.D. A heavy metal biotrap for wastewater remediation using poly- $\gamma$ -glutamic acid. *Biotechnol. Prog.* **2006**, *22*, 523–531. [[CrossRef](#)]
14. Wang, L.; Liu, Y.; Shu, X.; Lu, S.; Xie, X.; Shi, Q. Complexation and conformation of lead ion with poly- $\gamma$ -glutamic acid in soluble state. *PLoS ONE* **2019**, *14*, e0218742. [[CrossRef](#)]
15. Fei, Y.; Hu, Y.H. Design, synthesis, and performance of adsorbents for heavy metal removal from wastewater: A review. *J. Mater. Chem. A* **2022**, *10*, 1047–1085. [[CrossRef](#)]
16. Khan, M.; Lo, I.M.C. A holistic review of hydrogel applications in the adsorptive removal of aqueous pollutants: Recent progress, challenges, and perspectives. *Water Res.* **2016**, *106*, 259–271. [[CrossRef](#)]
17. ALSamman, M.T.; Sánchez, J. Recent advances on hydrogels based on chitosan and alginate for the adsorption of dyes and metal ions from water. *Arab. J. Chem.* **2021**, *14*, 103455. [[CrossRef](#)]
18. Samaddar, P.; Kumar, S.; Kim, K.-H. Polymer hydrogels and their applications toward sorptive removal of potential aqueous pollutants. *Polym. Rev.* **2019**, *59*, 418–464. [[CrossRef](#)]
19. Darban, Z.; Shahabuddin, S.; Gaur, R.; Ahmad, I.; Sridewi, N. Hydrogel-based adsorbent material for the effective removal of heavy metals from wastewater: A comprehensive review. *Gels* **2022**, *8*, 263. [[CrossRef](#)]
20. Perumal, S.; Atchudan, R.; Edison, T.N.J.I.; Babu, R.S.; Karpagavinayagam, P.; Vedhi, C. A short review on recent advances of hydrogel-based adsorbents for heavy metal ions. *Metals* **2021**, *11*, 864. [[CrossRef](#)]
21. Aoudi, B.; Boluk, Y.; El-Din, M.G. Recent advances and future perspective on nanocellulose-based materials in diverse water treatment applications. *Sci. Total Environ.* **2022**, *843*, 156903. [[CrossRef](#)] [[PubMed](#)]
22. Zhang, Y.; Zhao, M.; Cheng, Q.; Wang, C.; Li, H.; Han, X.; Fan, Z.; Su, G.; Pan, D.; Li, Z. Research progress of adsorption and removal of heavy metals by chitosan and its derivatives: A review. *Chemosphere* **2021**, *279*, 130927. [[CrossRef](#)] [[PubMed](#)]
23. Nangia, S.; Warkar, S.; Katyal, D. A review on environmental applications of chitosan biopolymeric hydrogel based composites. *Macromol. Rep.* **2018**, *55*, 747–763. [[CrossRef](#)]
24. Alves, D.C.d.S.; Healy, B.; Yu, T.; Breslin, C.B. Graphene-based materials immobilized within chitosan: Applications as adsorbents for the removal of aquatic pollutants. *Materials* **2021**, *14*, 3655. [[CrossRef](#)] [[PubMed](#)]
25. Chelu, M.; Musuc, A.M.; Popa, M.; Calderon Moreno, J.M. Chitosan hydrogels for water purification applications. *Gels* **2023**, *9*, 664. [[CrossRef](#)] [[PubMed](#)]

26. Yudaev, P.; Butorova, I.; Stepanov, G.; Chistyakov, E. Extraction of palladium(II) with a magnetic sorbent based on polyvinyl alcohol gel, metallic iron, and an environmentally friendly polydentate phosphazene-containing extractant. *Gels* **2022**, *8*, 492. [[CrossRef](#)] [[PubMed](#)]
27. Panic, V.V.; Velickovic, S.J. Removal of model cationic dye by adsorption onto poly(methacrylic acid)/zeolite hydrogel composites: Kinetics, equilibrium study and image analysis. *Sep. Purif. Technol.* **2014**, *122*, 384–394. [[CrossRef](#)]
28. Yang, Z.-H.; Dong, C.-D.; Chen, C.-W.; Sheu, Y.-T.; Kao, C.-M. Using poly-glutamic acid as soil-washing agent to remediate heavy metal-contaminated soils. *Environ. Sci. Pollut. Res.* **2018**, *25*, 5231–5242. [[CrossRef](#)]
29. Hisada, M.; Kawase, Y. Recovery of rare-earth metal neodymium from aqueous solutions by poly- $\gamma$ -glutamic acid and its sodium salt as biosorbents: Effects of solution pH on neodymium recovery mechanisms. *J. Rare Earths* **2018**, *36*, 528–536. [[CrossRef](#)]
30. Hisada, M.; Kawase, Y. Mucilage extracted from wasted natto (fermented soybeans) as a low-cost poly- $\gamma$ -glutamic acid based biosorbent: Removal of rare-earth metal Nd from aqueous solutions. *J. Environ. Chem. Eng.* **2017**, *5*, 6061–6069. [[CrossRef](#)]
31. Hajdu, I.; Bodnár, M.; Csikós, Z.; Wei, S.; Daróczy, L.; Kovács, B.; Gyóri, Z.; Tamás, J.; Borbély, J. Combined nano-membrane technology for removal of lead ions. *J. Membr. Sci.* **2012**, *409–410*, 44–53. [[CrossRef](#)]
32. Wang, F.; Zhao, J.; Wei, X.; Huo, F.; Li, W.; Hu, Q.; Liu, H. Adsorption of rare earths (III) by calcium alginate–poly glutamic acid hybrid gels. *J. Chem. Technol. Biotechnol.* **2014**, *89*, 969–977. [[CrossRef](#)]
33. Jin, X.; Liu, Y.; Tan, J.; Owens, G.; Chen, Z. Removing Cr(VI) from aqueous solutions via absorption by green synthesized PGA-PL-tannin gel. *Pol. J. Environ. Stud.* **2020**, *29*, 1973–1980. [[CrossRef](#)]
34. Duong, P.H.H.; Zuo, J.; Nunes, S.P. Dendrimeric thin-film composite membranes: Free volume, roughness, and fouling resistance. *Ind. Eng. Chem. Res.* **2017**, *56*, 14337–14349. [[CrossRef](#)]
35. Yang, S.; Fu, S.; Liu, H.; Zhou, Y.; Li, X. Hydrogel beads based on carboxymethyl cellulose for removal heavy metal ions. *J. Appl. Polym. Sci.* **2011**, *119*, 1204–1210. [[CrossRef](#)]
36. Mubark, A.E.; Hakem, H.A.; Zaki, E.G.; Elsaed, S.M.; Abdel-Rahman, A.A.-H. Sequestration of Cd(II) and Cu(II) ions using bio-based hydrogel: A study on the adsorption isotherms and kinetics. *Int. J. Environ. Sci. Technol.* **2022**, *19*, 10877–10892. [[CrossRef](#)]
37. Teow, Y.H.; Kam, L.M.; Mohammad, A.W. Synthesis of cellulose hydrogel for copper (II) ions adsorption. *J. Environ. Chem. Eng.* **2018**, *6*, 4588–4597. [[CrossRef](#)]
38. Chowdhury, M.N.K.; Ismail, A.F.; Beg, M.D.H.; Hegde, G.; Gohari, R.J. Polyvinyl alcohol/polysaccharide hydrogel graft materials for arsenic and heavy metal removal. *New J. Chem.* **2015**, *39*, 5823–5832. [[CrossRef](#)]
39. Romal, J.R.A.; Ong, S.K. Single-Step fabrication of a dual-sensitive chitosan hydrogel by c-mannich reaction: Synthesis, physico-chemical properties, and screening of its Cu<sup>2+</sup> uptake. *Processes* **2023**, *11*, 354. [[CrossRef](#)]
40. Dai, J.; Yan, H.; Yang, H.; Cheng, R. Simple method for preparation of chitosan/poly(acrylic acid) blending hydrogel beads and adsorption of copper(II) from aqueous solutions. *Chem. Eng. J.* **2010**, *165*, 240–249. [[CrossRef](#)]
41. Yan, H.; Dai, J.; Yang, Z.; Yang, H.; Cheng, R. Enhanced and selective adsorption of copper(II) ions on surface carboxymethylated chitosan hydrogel beads. *Chem. Eng. J.* **2011**, *174*, 586–594. [[CrossRef](#)]
42. Wu, X.; Wang, A.; Zheng, X.; Li, G.; Dong, X.; Wu, M. Study on optimal conditions and adsorption kinetics of copper from water by collodion membrane cross-linked poly- $\gamma$ -glutamic acid. *Korean J. Chem. Eng.* **2013**, *30*, 1295–1300. [[CrossRef](#)]
43. Chen, X.; Huang, Z.; Luo, S.-Y.; Zong, M.-H.; Lou, W.-Y. Multi-functional magnetic hydrogels based on *Milletia speciosa* Champ residue cellulose and Chitosan: Highly efficient and reusable adsorbent for Congo red and Cu<sup>2+</sup> removal. *Chem. Eng. J.* **2021**, *423*, 130198. [[CrossRef](#)]
44. Inbaraj, B.S.; Chen, B.-H. In vitro removal of toxic heavy metals by poly( $\gamma$ -glutamic acid)-coated superparamagnetic nanoparticles. *Int. J. Nanomed.* **2012**, *7*, 4419–4432. [[CrossRef](#)]
45. Inbaraj, B.S.; Chen, B.H. Dye adsorption characteristics of magnetite nanoparticles coated with a biopolymer poly( $\gamma$ -glutamic acid). *Bioresour. Technol.* **2011**, *102*, 8868–8876. [[CrossRef](#)] [[PubMed](#)]
46. Kolařík, J.; Bakandritsos, A.; Bad'ura, Z.; Lo, R.; Zoppellaro, G.; Kment, Š.; Naldoni, A.; Zhang, Y.; Petr, M.; Tomanec, O.; et al. Carboxylated graphene for radical-assisted ultra-trace-level water treatment and noble metal recovery. *Acs Nano* **2021**, *15*, 3349–3358. [[CrossRef](#)] [[PubMed](#)]
47. Huang, Z.; Liu, S.; Zhang, B.; Xu, L.; Hu, X. Equilibrium and kinetics studies on the absorption of Cu(II) from the aqueous phase using a  $\beta$ -cyclodextrin-based adsorbent. *Carbohydr. Polym.* **2012**, *88*, 609–617. [[CrossRef](#)]
48. Hamza, M.F.; Wei, Y.; Guibal, E. Quaternization of algal/PEI beads (a new sorbent): Characterization and application to scandium sorption from aqueous solutions. *Chem. Eng. J.* **2020**, *383*, 123210. [[CrossRef](#)]
49. Stevens, J.S.; Luca, A.C.d.; Pelendritis, M.; Terenghi, G.; Downes, S.; Schroeder, S.L.M. Quantitative analysis of complex amino acids and RGD peptides by X-ray photoelectron spectroscopy (XPS). *Surf. Interface Anal.* **2013**, *45*, 1238–1246. [[CrossRef](#)]
50. Ding, J.; Zhang, C.; Zhang, J.; Liu, H.; Yu, G.; Yu, T.; Wang, Y.; Guo, X.; Ding, J.D.J.D.J.; Zhang, C.Z.C.Z.C.; et al. Comparative study on CuO–La<sub>2</sub>O<sub>3</sub>/ZrO<sub>2</sub> catalysts prepared by amino acid complexing-combustion in CO<sub>2</sub> hydrogenation. *Asia-Pac. J. Chem. Eng.* **2023**, *18*, e2879. [[CrossRef](#)]

**Disclaimer/Publisher's Note:** The statements, opinions and data contained in all publications are solely those of the individual author(s) and contributor(s) and not of MDPI and/or the editor(s). MDPI and/or the editor(s) disclaim responsibility for any injury to people or property resulting from any ideas, methods, instructions or products referred to in the content.